ACS Catalysis

Research Article

pubs.acs.org/acscatalysis

# Mechanistic Insights on Sulfide-Adsorption Enhanced Activity of Methanol Electro-Oxidation on Pt Nanoparticles

In-Su Park,[†,‡] Dianne Osena Atienza,[†] Augusta M. Hofstead-Duffy,[†] Dejun Chen,[†] and YuYe J. Tong*[,†]

[†]Department of Chemistry, Georgetown University, Washington, D.C. 20057, United States

[‡]Mineral Resources Research Division, Korea Institute of Geoscience and Mineral Resources, Yuseong-gu, Daejeon 305-350, Korea

Supporting Information

**ABSTRACT:** The effect of adsorbed sulfide ($S^{2-}{}_{ads}$) on methanol (MeOH) electro-oxidation reaction (MOR) taking place on carbon-supported Pt nanoparticles (NPs) was investigated using electrochemical and attenuated-total-reflection (ATR)-FTIR spectroscopic techniques. The observed substantial enhancement in MOR activity per active site was rationalized by an enhanced parallel reaction pathway by the $S^{2-}$ adsorption that did not lead to poisonous CO. Moreover, there were delayed/suppressed adsorption of electrolyte anions and oxygen-containing species and increased amount of isolated free water monomers caused by the sulfide adsorption-induced more negatively charged Pt sites, which led to more available active sites, weakened bonding interaction between the Pt NPs and oxygen-containing species, and more active water species for MOR along the parallel reaction pathway.

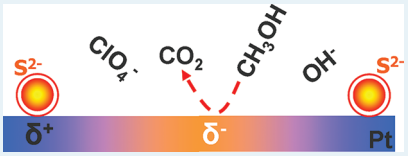


**KEYWORDS:** *Pt electrocatalyst, sulfide adsorption, enhanced methanol electro-oxidation, parallel reaction pathway*

## INTRODUCTION

Adsorption of sulfur (S)-containing molecules on Pt has attracted much interest in heterogeneous catalysis in general and electrocatalysis in particular. This is largely due to its frequently observed strong negative effect on the catalytic activity.[1,2] Strongly adsorbed S ($S_{ads}$) on Pt in solid/gas system induces a significant depletion in the 5d population of Pt through predominantly covalent bonding, which causes a large reduction in the density of states of Pt around the Fermi level.[3] Accordingly, the $S_{ads}$ on Pt significantly affects the reactivity of the Pt surface toward small molecules (CO, $H_2$, $C_2H_4$, etc.) through the modified reactant-Pt interaction and lateral interaction between adsorbates.[4,5] For instance, $S_{ads}$ on Pt (111) reduces the adsorption energy of CO by ~8 kcal/mol, ascribed to a S-induced weakening in the Pt-CO($2\pi^*$) bonding interactions.[6] Additionally, the repulsive $S_{ads}$↔CO interactions also reduce the adsorption strength and diffusion rate of CO on Pt surface, and compress local S coverage, which eventually lead to the formation of molecular polysulfur ($S_n$) species.[7]

In electrocatalysis, the $S_{ads}$ effects on Pt reactivity are different, depending on the specific electrocatalytic reaction. Recent studies have shown that the $S_{ads}$ on Pt nanoparticles (NPs) substantially impedes the oxygen reduction reaction (ORR) and hydrogen oxidation reaction.[8,9] In particular, it was observed that $S_{ads}$ enhances the formation of deleterious $H_2O_2$ byproduct during the ORR. On the other hand, some early studies showed that the S adsorption on Pt enhances activity in formic acid, formaldehyde, and methanol (MeOH) electro-oxidation reactions.[10−13] For instance, $S_{ads}$-Pt demonstrates an increased adsorption rate constant of the reactants in formic acid electro-oxidation reaction, in which the observed activity also shows a strong S-coverage ($\theta_S$) dependence.[10,13,14] Several mechanisms have been proposed to explain such opposing effects, which include the entropy effect,[10] chemical state effect,[12] site-modifying effect, and site-blocking effect,[13] just to name a few. As to the observation of increased cathodic currents in the hydrogen adsorption region after S adsorption, it was interpreted as a decrease in the amount of hardly reducible Pt oxides by $S_{ads}$[13] or the reversible hydrogenation of S sites.[11] On the other hand, spectroscopic analysis suggested that $S_{ads}$ on Pt is mainly in an atomic state, but with a partial negative charge.[12,15,16] Consequently, the decreased bonding energy of adsorbed hydrogen on $S_{ads}$-Pt was attributed to the S-induced local electronic deficit on Pt[16] while a suppressed electro-oxidation of 1,3-butanediol on $S_{ads}$-Pt was interpreted in terms of the negatively charged $S_{ads}$-Pt surface.[17] Clearly, no consensus has emerged to date.

Most recently, we have investigated the chemical state of $S_{ads}$ on commercial Pt black and carbon-supported NPs by a combination of detailed electrochemical (EC) measurements, in situ surface enhanced Raman scattering (SERS) study, and ab initio density functional theory (DFT) calculations using the polarizable continuum model (PCM).[18] The SERS data of the $S_{ads}$ coupled with the DFT calculations provided the convincing evidence showing that the $S_{ads}$ was in a sulfide ($S^{2-}$) state, consistent with S having a much higher electron-affinity than Pt.[19] Such a sulfide ($S^{2-}$) state of $S_{ads}$ may strongly influence the EC oxidation of small organic molecules similar to adsorbed anions.[20−22] Equipped with this improved understanding of the chemical state of $S_{abs}$ at a solid/liquid interface, we set out to examine the mechanistic effect of the adsorbed sulfide ($S^{2-}{}_{ads}$)

Received: October 24, 2011
Revised: November 19, 2011
Published: November 28, 2011

  

on the MeOH electro-oxidation reaction (MOR), which are reported herein.

## RESULTS AND DISCUSSION

Figure 1a shows the cyclic voltammograms (CVs) for MOR on clean and $S^{2-}$-adsorbed carbon supported Pt NPs (see Experimental Section for details). The current density ($j$) was obtained by normalizing the reaction current by the clean surface areas before $S^{2-}$ deposition (hydrogen desorption charges, 0.21 mC/cm$^2$).[23] Surprisingly, despite a decrease in the surface area unoccupied by $S^{2-}{}_{ads}$, the Pt NPs having a sulfide coverage of $\theta_{S,H}$ = 0.24 and 0.52 still showed higher current density $j$ values than that of the clean Pt NPs above the onset potential. Here $\theta_{S,H}$ was calculated by $1 - Q_{S,H}/Q_{clean,H}$ where $Q_{S,H}$ and $Q_{clean,H}$ were the hydrogen desorption charge with and without adsorbed $S^{2-}$, respectively. Quantitatively, this enhancement was illustrated by comparing the anodic current density $j_{0.31\ V}$ at 0.31 V, a potential that is relevant to MeOH fuel cell application, as shown in Figure 1b (left $y$-axis). To further illustrate the intrinsic effect of $S^{2-}{}_{ads}$, an enhancement factor $\eta$ defined as $\eta = j_s/[(1 - \theta_{S,H})\cdot j_{Pt}]$, where $j_{Pt}$ and $j_S$ are the anodic current densities for clean and $S^{2-}{}_{ads}$-Pt NPs, respectively ($j_S = j_{Pt}$ when $\theta_{S,H} = 0$), was calculated from currents at 0.31 V in Figure 1a. In other words, $\eta$ is the ratio of current densities normalized by the respective unblocked Pt surface area. As shown in Figure 1b (right $y$-axis), the $\eta$ increased linearly as a function of $\theta_{S,H}$ in the $\eta$ in logarithmic scale versus $\theta_{S,H}$ plot, clearly illustrating the intrinsic enhancement of MOR by $S^{2-}{}_{ads}$.

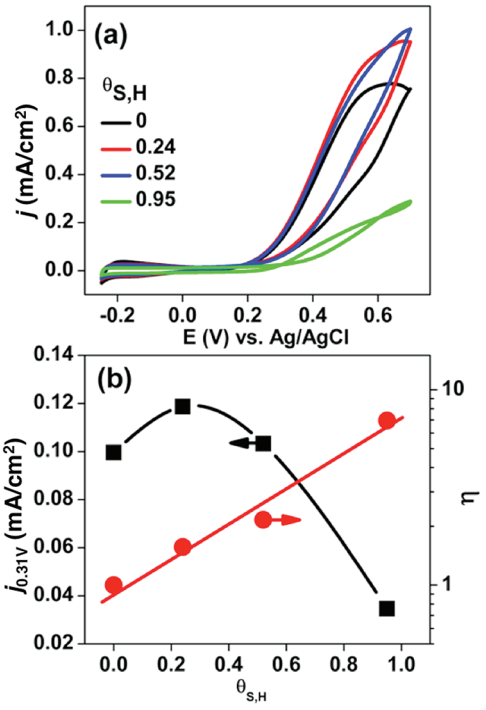


**Figure 1.** (a) CV profiles for MOR and (b) the current density ($j_{0.31\ V}$) and enhancement factor ($\eta$) vs $S^{2-}$ coverage ($\theta_{S,H}$) measured at 0.31 V. The CVs were obtained using 50 mV/s of scan rate. The $S^{2-}$ coverage ($\theta_{S,H}$) was calculated using $\theta_{S,H} = 1 - (Q_{S,H}/Q_{clean,H})$, where $Q_{S,H}$ and $Q_{clean,H}$ are hydrogen (H) desorption charges for the clean and $S^{2-}{}_{ads}$-Pt NPs, respectively.

In a steady state condition at low temperature and low potentials, MOR on Pt follows primarily the indirect reaction pathway via the formation of CO that is eventually oxidized to $CO_2$ by the surface reaction with adsorbed OH ($OH_{ads}$) according to the Langmuir–Hinshelwood mechanism.[24,25] That is, the electrocatalytic activity of MOR is determined by the accumulation rate of adsorbed CO ($CO_{ads}$) formed during MOR and its oxidation rate into $CO_2$. Therefore, information on poisoning intermediates (PIs) formed during MOR would provide more mechanistic insights on the enhancement effect of $S^{2-}{}_{ads}$ on MOR. The following experiments were carried out to achieve this goal.[26]

The first step was a chronoamperometric (CA) measurement at a reaction potential $E_r$ for a given reaction time $t_r$ during which accumulative reaction charge density $q_r$ was measured. At the end of this time, the potential was stepped to −0.24 V, at which a rinsing procedure was carried out to remove MeOH, but kept the generated PIs intact (see Experimental Section). Immediately after the rinsing procedure, a PIs stripping CV was taken, from which the amount of charge density for the PIs oxidation, $q_{PI}$ was obtained. Figure 2 shows the results for data obtained at $E_r$ = 0.31 V on the clean Pt sample: CV curves of $t_r$ = 100, 600, and 1800 s, respectively (a), the corresponding PIs stripping CV (b), $q_r$'s (c), and $q_{PI}$'s (d), respectively. The $q_r$ and $q_{PI}$ were obtained using the area calculated from the hydrogen desorption charge of the second PIs stripping CV as the normalization factor. The $q_r$ showed a linear relationship with reaction time $t_r$ in a log–log plot (Figure 2c), similar to those observed on Pt(111).[27,28] The $q_{PI}$ (0.150 mC/cm$^2$ ± 0.005), however, was constant for different $t_r$, which indicated that the MOR reaction at 0.31 V had already reached the steady state at a reaction time as short as 100 s. The accuracy and reproducibility of the PIs analysis on the Pt NPs were ensured by running at least two independent runs of measurements. Notice that the redox peaks in Figure 2b at 0.36/0.32 V as indicated by the arrows came from the redox of the oxygen-containing

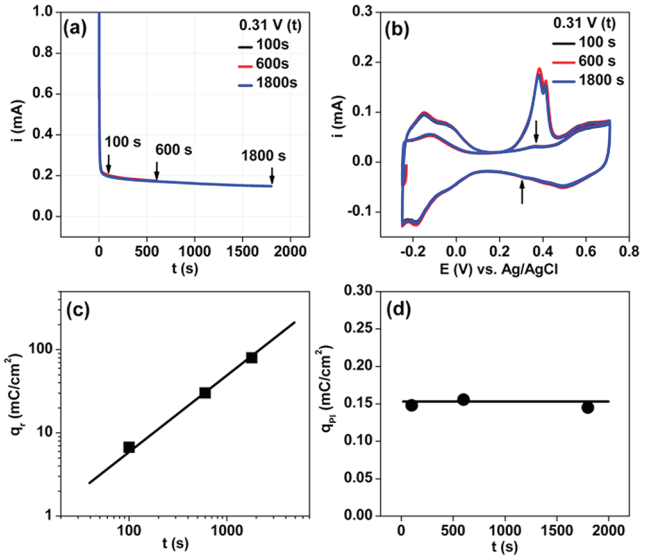


**Figure 2.** (a) Current (i)-reaction time ($t$) curves of the clean Pt NPs measured at 0.31 V with different reaction time (100 s, 600 s, 1800 s), (b) the PI stripping CV profiles obtained using 20 mV/s of scan rate, (c) the reaction charge density ($q_r$) vs reaction time ($t$), and (d) the PI stripping charge density ($q_{PI}$) vs reaction time ($t$).


dx.doi.org/10.1021/cs200546f | ACS Catal. 2012, 2, 168–174

groups (mainly quinone) of the carbon support surface.[29] Its current contribution to $q_{PI}$ was minor (ca. 0.03%) so can be safely neglected for our analyses.

The above $q_r$ and $q_{PI}$ analyses at $t_r$ = 100 s were carried out for all samples as a function of reaction potential $E_r$ (0.01 V ≤ $E_r$ ≥ 0.46 V). The corresponding results are presented in Figure 3a

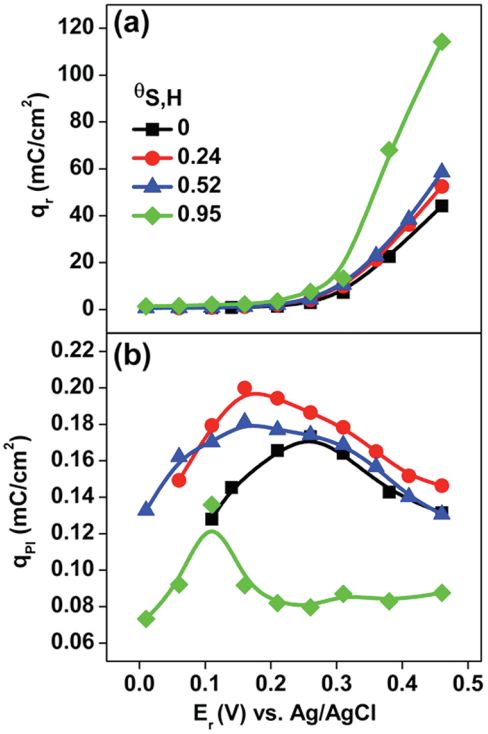


**Figure 3.** Reaction charge density ($q_r$) (a) and the PI charge density ($q_{PI}$) (b) vs $E_r$ curves.

and 3b. The original data are collected in Supporting Information, Figures S1 and S2. Notice that for the $\theta_{S,H}$ = 0.95 sample, double layer charging and redox peaks of quinone-like species had a significant presence in the PIs stripping curves (Supporting Information, Figure S2d). To reduce the uncertainty, the $q_{PI}$ was obtained after subtraction of the second from the first PIs stripping CV, and the $q_r$ was corrected using current density at −0.24 V (before applying the reaction potential). As shown in Figure 3a, all the $S^{2-}_{ads}$-Pt samples demonstrated an enhanced activity as compared to the clean Pt sample at potentials above $E_r$ = 0.15 V as measured by $q_r$. On the other hand, the $q_{PI}$ versus $E_r$ curves in Figure 3b shows strong $E_r$ and $\theta_{S,H}$ dependence. Every curve has a peak whose position varies as the $\theta_{S,H}$ changes, reflecting the fact that the PIs started accumulating at lower potentials, but being oxidized away at high potentials. The $\theta_{S,H}$ = 0.95 sample has the lowest peak potential (0.1 V), followed by the $\theta_{S,H}$ = 0.52 (0.16 V) and 0.24 (0.18 V), and last by the clean Pt sample (0.26 V). The lower peak potentials for S-adsorbed samples suggest that the PIs could be oxidized earlier on these samples, implying higher PI tolerance thus higher activities as observed. Notwithstanding, the amount of PIs generated on the $\theta_{S,H}$ = 0.24 and 0.52 samples (the values at peak $q_{PI}^{peak}$ = 0.20 mC/cm$^2$ and 0.18 mC/cm$^2$ respectively) were higher than that (0.17 mC/cm$^2$) on the clean Pt sample, particularly at lower potentials (the solid circles and triangle vs squares in Figure 3b). Notice that the $q_{PI}^{peak}$ = 0.17 mC/cm$^2$ for the clean Pt sample was almost the same as that (0.16 mC/cm$^2$) of the polyoriented Pt surface,[30] giving confidence to the reliability of our data analysis.

To shed light on the increased PIs generation on the $S^{2-}_{ads}$-Pt NPs during MOR, the yields ($y_{PI}$) of the PIs products were analyzed using the method developed by Stuve and co-workers[26] by assuming that $CO_2$ and CO are the complete and PI products. This leads to the following equation: $y_{PI} = 3q_{PI}/(q_r + q_{PI})$. The calculated results were presented in Figure 4,

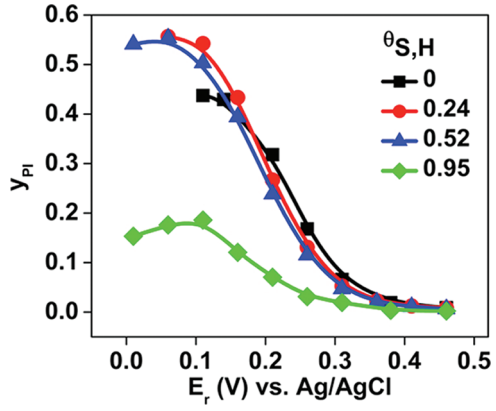


**Figure 4.** Yield of PI product ($y_{PI}$) vs $E_r$ curves, which were calculated by $y_P = 3q_{PI}/(q_r + q_{PI})$. See the text for details.

from which several interesting observation can be made. First, all $y_{PI}$ values were less than 1 with the highest value ~0.55 and decreased as $E_r$ increased. This suggests strongly that at least one non-negligible parallel reaction pathways was operational and eventually became dominant as $E_r$ increased. Second, the $y_{PI}$ values were larger on the $\theta_{S,H}$ = 0.24 and 0.52 samples than on the clean Pt when $E_r$ < 0.15 V, but became smaller when $E_r$ > 0.15 V. These results imply that the enhanced MOR activity as observed in Figure 1 came largely from the enhancement in the parallel reaction pathway, at least for $E_r$ < 0.4 V below which the majority of adsorbed CO would be intact (see Figure 5). Third, increasing S coverage increased the percentage

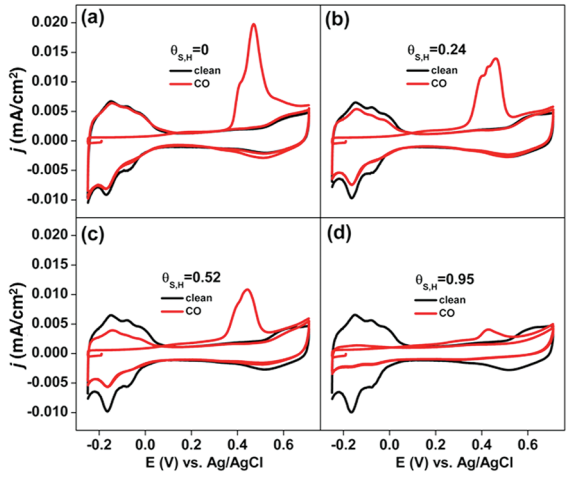


**Figure 5.** Clean surface (black) and CO stripping (red) CV profiles of samples having different $S^{2-}$ coverages: (a) $\theta_{S,H}$ = 0, (b) $\theta_{S,H}$ = 0.24, (c) $\theta_{S,H}$ = 0.52, and (d) $\theta_{S,H}$ = 0.95. The CVs were obtained using 5 mV/s of scan rate.

of contribution to the total reaction current from the parallel reaction pathway.


dx.doi.org/10.1021/cs200546f | ACS Catal. 2012, 2, 168–174

The effect of $S^{2-}{}_{ads}$ on the catalytic behavior of the Pt NPs was further investigated by gaseous CO monolayer oxidation. Figure 5 shows the consecutive CO stripping CV profiles (1st and second) and the corresponding CV for the clean surfaces before $S^{2-}$ adsorption. The current density ($j$) was obtained by normalizing the currents by the clean surface area (without $S^{2-}{}_{ads}$). The CO stripping profiles show clearly observable preoxidation current that may correspond to oxidizing weakly adsorbed species at low potential region and main peaks (oxidizing strongly adsorbed state) at high potential region. The sulfide adsorption enhanced the former but suppressed the latter with increasing S coverage. Figure 6a shows a linear

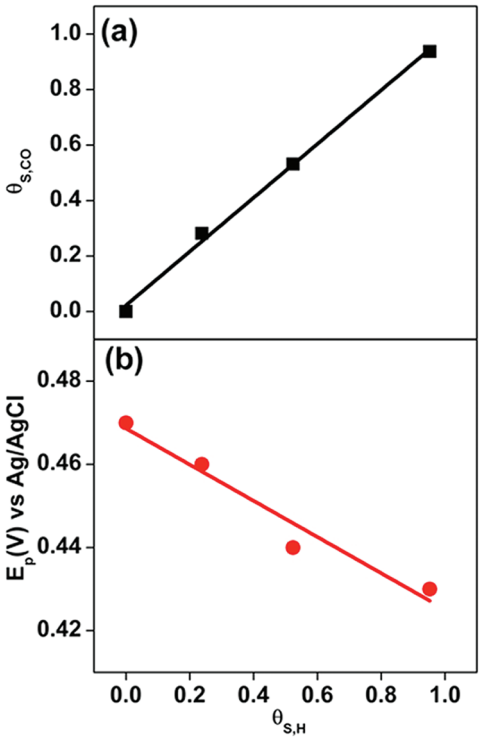


**Figure 6.** CO-stripping determined $S^{2-}$ coverage ($\theta_{S,CO}$) (a) and $E_p$ (V) (b) vs hydrogen-desorption determined S coverage ($\theta_{S,H}$) plots. The $E_P$ indicates the potential for maximum current in CO stripping.

relationship between $\theta_{S,H}$ and $\theta_{S,CO}$. The latter was calculated by $1 - Q_{S,CO}/Q_{clean,CO}$ where $Q_{S,CO}$ and $Q_{clean,CO}$ were the CO stripping charge with and without adsorbed $S^{2-}$, respectively. The latter were calculated from the CO oxidation charges obtained in Figure 5. The linear relationship indicates that a similar long-range interaction between $S^{2-}{}_{ads}$ and CO adsorption as between $S^{2-}{}_{ads}$ and H adsorption. Also plotted in Figure 6b is the potential ($E_p$) for maximum CO stripping current as a function of S coverage. The negative shift of the potential as the S coverage increased implies an easier CO electro-oxidation, thus an improved CO tolerance by S adsorption.

Further insights can be gleaned by looking at how S adsorption affects the behavior of electrolyte anions adsorption, such as $ClO_4^-$ adsorption in this study. Figure 7a compared the in situ IR spectra of the clean Pt and $\theta_{S,H}$ = 0.57 samples obtained by attenuated-total-reflection (ATR) surface-enhanced IR reflection absorption spectroscopy (SEIRAS) using the stairs-step method.[31] As can be seen, the clean Pt NPs show two bands associated with the 2-fold (1164 $cm^{-1}$) and one-fold (1100 $cm^{-1}$)

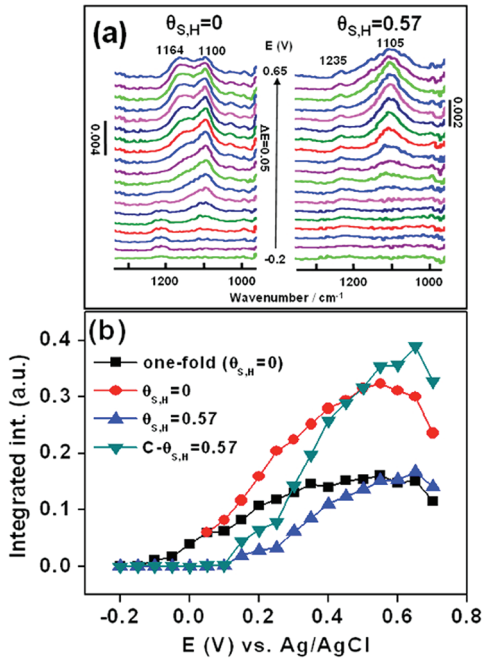


**Figure 7.** (a) FT-IR spectra of anion $ClO_4^-$ at different $S^{2-}$ coverage ($\theta_{S,H}$) and (b) integrated intensities vs $E$ (V) plot. The C in (b) indicates the $\theta_{S,H}$-corrected integrated intensity, i.e., normalized by $(1 - \theta_{S,H})$.

adsorption modes of $ClO_4^-$.[32−34] As the electrode potential increased, the anion adsorption increased too as expected. Interestingly, for the S-adsorbed Pt sample ($\theta_{S,H}$ = 0.57), not only was the 2-fold adsorption mode for $ClO_4^-$ largely suppressed, but also was the anion adsorption delayed significantly. Figure 7b presents the IR band integrals as a function of electrode potential. For the clean Pt sample, the anion band showed up at a potential as low as −0.15 V, but not until 0.1 V for the S-adsorbed sample. Furthermore, the amount of adsorbed anions was significantly lower on the S-adsorbed sample than on the clean Pt sample in the potential region <0.4 V. On the other hand, the IR measurements showed that the S-absorption had a very weak effect on water bending vibration (Supporting Information, Figure S3) but strong effect on water stretching vibrations (Supporting Information, Figure S4). The S coverage-corrected band integrals of the water bending vibration at 1612 $cm^{-1}$ almost overlap with those (also at 1612 $cm^{-1}$) of the clean Pt NPs below 0.5 V, suggesting the total amount of surface water did not change too much. On the clean Pt NPs, the decrease in the IR band integrals for both anion and water adsorption over 0.5 V is ascribed to the strong adsorption of oxygenated species, that is, OH. Thus, the continuous increase in the IR band integrals of adsorbed anions (Figure 7b) and water (Supporting Information, Figure S3b) beyond 0.5 V on the $S^{2-}{}_{ads}$-Pt NPs suggests that the S-adsorption suppressed/delayed the OH adsorption. Intriguingly, the water stretching bands revealed interesting changes. Two stretching bands corresponding to strongly hydrogen-bound water (3226 $cm^{-1}$) and isolated free water monomers (3602 $cm^{-1}$) were observed.[31] For the Pt/C without sulfide adsorption, the strongly hydrogen-bound water dominated (Supporting Information, Figure S4b). But for the Pt/C with sulfide adsorption, isolated free water monomers dominated instead (Supporting Information, Figure S4c). Such change


dx.doi.org/10.1021/cs200546f | ACS Catal. 2012, 2, 168−174

may also affect the MOR activity if the latter water species were an active participant for the parallel reaction pathway.

Because of the negative charge carried by the adsorbed sulfide, surface charge is expected to vary noticeably as the S coverage changes. We used the CO-displacement method[35,36] to determine the pztc (potential of zero total charge) values as a function of $S^{2-}$ coverage as a way to quantify it. The total surface charge $q$ versus $E$ curves were obtained by integration of the voltammetric current, corrected for the double layer current because of the larger-than-usual values for carbon-supported Pt NPs:

$$q(E) = \int \frac{j - j_{dl}}{\nu} \, dE - q_{dis}(E^*)$$

where $j$, $j_{dl}$, $\nu$, and $q_{dis}(E^*)$ are the total current density, current density at double region, scan rate, and displaced charge density, respectively. As shown in Figure 8, the pztc of the

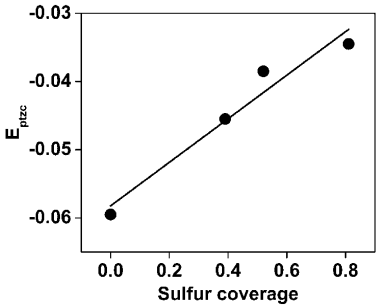


**Figure 8.** $E_{pztc}$ vs $\theta_{S,H}$ plot. The total surface charge $q(E)$ versus $E$ curves by which the $E_{pztc}$ values were determined ($q(E_{ptzc}) = 0$) were obtained by integration of the voltammetric current after correction of double layer current.

$S^{2-}{}_{ads}$-Pt NPs, determined by $q(E_{ptzc}) = 0$, shifted positively as the $\theta_{S,H}$ increased, implying a more and more negatively charged Pt surface as the S coverage increased, which is consistent with our identification of sulfide ($S^{2-}$) as the adsorbed S species on Pt surface.

It is expected that the presence of $S^{2-}$ would bring a substantial amount of electron density between the adsorbed $S^{2-}$ and the hosting Pt site and the associated repulsive electrostatic interaction would push electrons more onto $S^{2-}$-unoccupied Pt surface sites where surface reaction would take place. This would increase the overall tendency of the surface to repel negatively charged species and explain the delayed/suppressed anion adsorption and the adsorption of usually negatively charged oxygen-containing species. On the other hand, the PIs analysis of MOR on the $S^{2-}$-adsorbed Pt NPs indicates that $S^{2-}$ adsorption induced the generation of higher amount of PIs at low electrode potentials, which implied the enhanced decomposition rate of MeOH to PIs. The C−H bond split is known as the rate-determining step in the overall MeOH decomposition process[37] and the $CH_3$ group is the positive pole of the dipolar MeOH molecule. Thus, the increased negatively charged surface by $S^{2-}$ adsorption would increase its attraction to the $CH_3$ group by which the decomposition of MeOH would be enhanced, leading to higher $q_{PI}$ values on the $\theta_{S,H}$ = 0.24 and 0.52 samples than on the clean Pt sample (Figure 3b). This may also explain substantially increased amount of isolated free water monomers: The positive pole of water (hydrogen) was attracted strongly toward the negative charged surface that eventually broke the initially dominating hydrogen bonds. On the other hand, the $S^{2-}$ adsorption also enhanced the parallel reaction pathway (Figure 4). Although the exact mechanism by which $S^{2-}$ adsorption enhances the parallel reaction pathway and what steps are involved in this parallel reaction pathway remain elusive; these questions are currently under investigation. The delayed/suppressed anion adsorption and the adsorption of oxygen-containing species would imply more available sites and weakened bonding interaction between the oxygen-containing species and the Pt NP surface at the electrode potentials of interest. We speculate that these two effects would synergistically enhance the parallel reaction pathway. Additionally, the increased amount of water monomers may also play a role.

## CONCLUSIONS

We have reported a mechanistic investigation of the enhanced MOR activity on carbon supported Pt NPs induced by the adsorption of sulfide by EC and in situ ATR-SEIRAS techniques. We were able to obtain two major insightful observations into how S adsorption affects MOR on Pt NPs. First, the enhanced intrinsic MOR activity per available site by S adsorption was largely due to the enhanced parallel reaction pathway that did not generate poisonous CO (Figure 4), and the percentage of the contribution to the total reaction current from the parallel reaction pathway increased proportionally to the $S^{2-}$ coverage (Figure 4). Second, the more negatively charged Pt surface brought to bear by the adsorbed sulfide ($S^{2-}$) delayed/suppressed the adsorption of anions and oxygen-containing species (Figure 7 and Supporting Information, Figure S3) lead to more available Pt sites for reaction and weakened bonding interaction between the oxygen-containing species and the Pt NP surface, which would enhance synergistically the parallel reaction pathway. The sulfide adsorption also increased the amount of isolated free water monomers on the surface by breaking the initially dominating hydrogen bonds, which could also play a role in enhancing the parallel reaction pathway. The exact mechanism, however, by which $S^{2-}$ adsorption enhances the parallel reaction pathway of MOR on Pt and the exact steps in the parallel reaction pathway are still elusive. Thus, further investigations are highly warranted and are currently underway in our lab.

## EXPERIMENTAL SECTION

**Adsorption of S on Pt NPs.** The adsorbed S structure formed spontaneously on carbon-supported Pt NPs (40 wt.% Pt/C, $d \sim 4.13$ nm, J-M). The Pt/C (2.5 mg) was mixed with DI-water (25 $\mu$L), IPA (965 $\mu$L) and Nafion solution (5 wt.%, 10 $\mu$L). The mixture was then sonicated for at least 10 min to form a uniform suspension. The 10 $\mu$L of mixture was drop-cast onto a glassy carbon (GC, 3 mm diameter, Bioanalytical) electrode. Before Pt/C loading, the GC was polished using alumina powder, and its clean surface was confirmed by the CVs. The Pt-loaded electrode was air-dried and rinsed with a Milli-Q water (18.2 MΩ·cm). The $S^{2-}{}_{ads}$-Pt NPs were prepared by immersing a Pt/C-loaded electrode in 1 mM $Na_2S$ solution using different deposition time ($t$ < 1200 s). The S solutions were prepared just before each series of measurements. Before S deposition, the clean Pt surface was prepared in 0.1 M $HClO_4$ solution by multicycling (30 CVs) using potential region (−0.25−1.2 V vs Ag/AgCl) and scan rate (50 mV/s).


dx.doi.org/10.1021/cs200546f | ACS Catal. 2012, 2, 168−174

**Electrochemical Measurement.** All EC experiments were carried out in a conventional three-electrode EC cell using a CHI 760C EC workstation (CHI Instrument) with CHI760 software. The GC electrode, Pt gauze, and Ag/AgCl (3M) (Bioanalytical) were used as working, counter, and reference electrode, respectively. All CVs were recorded in 0.1 M $HClO_4$ or 0.5 M $H_2SO_4$ solutions under an aerobic environment. For MOR, 200 $\mu$L of MeOH was added into the 10 mL of Ar-purged electrolyte at −0.24 V, and the CVs were obtained using 50 mV/s. For experiments on the poisoning intermediates (PIs) generated during MOR, identical two EC cells (*A* and *B*) were used for MOR and the rinsing process of the electrode under a constant potential (−0.24 V). The $S^{2-}_{ads}$-Pt NPs were immersed into cell *A* that contained blank electrolyte, and the CV was obtained using 20 mV/s of scan rate. After this, the 200 $\mu$L of MeOH was added to the 10 mL of Ar-purged electrolyte at −0.24 V and then *i*−*t* curve was obtained at the reaction potential ($E_r$) for a duration of reaction time ($t$). After *i*−*t* curve measurement, the Ar bubbling was performed for 30 min at −0.24 V as the first rinsing process, followed by transferring the electrode to cell *B* that contained blank electrolyte. After rinsing the electrode in cell *B*, the electrode was transferred back to cell *A* that now also contained blank electrolyte, and a second rinsing process was performed using the same condition in cell *B*. For the PIs stripping, the CV was obtained using 20 mV/s of scan rate after rinsing the electrode in cell *A*. For CO stripping, CO adsorption was performed at −0.19 V with CO purging for 5 min followed by Ar purging for 10 min. CVs were then obtained using 5 mV/s of scan rate under an Ar-blanket.

**In Situ ATR-FTIR Spectroscopy.** All SEIRAS data acquisitions were carried out on a Bruker Vector-22 Fourier transform IR spectrometer equipped with a liquid-nitrogen-cooled mercury−cadmium-telluride (MCT) detector. An EC-IR cell with a triangular Si prism and an optical reflection accessory (incident angle of >60° enabling total attenuation reflection) were both home-built. The spectral resolution was 4 $cm^{-1}$. The obtained spectra were shown in the absorbance units defined as $-\log(I/I_0)$ where $I$ and $I_0$ are the single-beam spectral intensities at the measuring potential and the reference potential, respectively. The total number of added spectra for each potential is 100 scans. A gold film was electrolessly deposited onto the reflecting plane of a Si attenuation total reflection (ATR) prism of a triangular shape, which was polished with successively finer grade alumina slurries down to 0.3 $\mu$m and cleaned by sonication in the Milli-Q water. The detailed deposition procedure can be found elsewhere.[38] The DI-water dissolved Pt/C was dropped on gold film and dried at room temperature. To avoid any optical interference, no Nafion solution was used. The $S^{2-}_{ads}$-Pt NPs on gold film were prepared by exposing them to $Na_2S$ solution and washed with clean DI water.

## ■ ASSOCIATED CONTENT

### Supporting Information

Further details are given in Figures S1−S4. This material is available free of charge via the Internet at http://pubs.acs.org.

## ■ AUTHOR INFORMATION

### Corresponding Author

*Phone: +1-202-687-5872. Fax: +1-202-687-5591. E-mail: yyt@georgetown.edu.

### Funding

The authors gratefully acknowledge the financial support by from DOE (DE-FG02-07ER15895). D.J.C. is supported partially by a scholarship from the Chinese Scholar Council.

## ■ REFERENCES

(1) Jerkiewicz, G.; Borodzinski, J. J.; Chrzanowskia, W.; Conway, B. E. *J. Electrochem. Soc.* **1995**, *142*, 3755.
(2) Sethuraman, V. A.; Weidner, J. W. *Electrochim. Acta* **2010**, *55*, 5683.
(3) Billy, J.; Abon, M. *Surf. Sci.* **1984**, *146*, L525.
(4) Rodriguez, J. A.; Kuhn, M.; Hrbek, J. *Chem. Phys. Lett.* **1996**, *251*, 13.
(5) Rodriguez, J. A.; Hrbek, J. *Acc. Chem. Res.* **1999**, *32*, 719.
(6) Kiskinova, M.; Szabo, A.; Yates, J. T. *J. Chem. Phys.* **1988**, *89*, 7599.
(7) Batteas, J. D.; Dunphy, J. C.; Somorjai, G. A.; Salmeron, M. *Phys. Rev. Lett.* **1996**, *77*, 534.
(8) Garsany, Y.; Baturina, O. A.; Swider-Lyons, K. E. *J. Electrochem. Soc.* **2007**, *154*, B670.
(9) Pietron, J. J. *J. Electrochem. Soc.* **2009**, *156*, B1322.
(10) Jayaram, R.; Contractor, A. Q.; Lal, H. *J. Electroanal. Chem.* **1978**, *87*, 225.
(11) Contractor, A. Q.; Lal, H. *J. Electroanal. Chem.* **1979**, *103*, 103.
(12) Sun, S.-G.; Chen, S.-P.; Li, N.-H.; Lu, G.-Q.; Chen, B.-Z.; Xu, F.-C. *Colloids Surf., A* **1998**, *134*, 207.
(13) Loucka, T. *J. Electroanal. Chem.* **1972**, *36*, 355.
(14) Loucka, T. *J. Electroanal. Chem.* **1972**, *36*, 369.
(15) Sung, Y. E.; Chrzanowski, W.; Zolfaghari, A.; Jerkiewicz, G.; Wieckowski, A. *J. Am. Chem. Soc.* **1997**, *119*, 194.
(16) Zolfaghari, A.; Jerkiewicz, G.; Chrzanowski, W.; Wieckowski, A. *J. Electrochem. Soc.* **1999**, *146*, 4158.
(17) Wu, Q.-H.; Li, N.-H.; Sun, S.-G. *J. Phys. Chem. B* **2006**, *110*, 11383.
(18) Park, I.-S.; Xu, B.; Atienza, D. O.; Hofstead-Duffy, A. M.; Allison, T. C.; Tong, Y. Y. J. *ChemPhysChem* **2011**, *12*, 722.
(19) Herrero, E.; Climent, V.; Feliu, J. M. *Electrochem. Commun.* **2000**, *2*, 636.
(20) Schmidt, T. J.; Grgur, B. N.; Markovic, N. M.; Ross, P. N. *J. Electroanal. Chem.* **2001**, *500*, 36.
(21) Santos, M. C.; Miwa, D. W.; Machado, S. A. S. *Electrochem. Commun.* **2000**, *2*, 692.
(22) Chen, S.; Noles, T.; Schell, M. *J. Phys. Chem. A* **2000**, *104*, 6791.
(23) Pozio, A.; De Francesco, M.; Cemmi, A.; Cardellini, F.; Giorgi, L. *J. Power Sources* **2002**, *105*, 13.
(24) Markovic, N. M.; Schmidt, T. J.; Grgur, B. N.; Gasteiger, H. A.; Behm, R. J.; Ross, P. N. *J. Phys. Chem. B* **1999**, *103*, 8568.
(25) Neurock, M.; Janik, M.; Wieckowski, A. *Faraday Discuss.* **2008**, *140*, 363.
(26) Jarvi, T. D.; Sriramulu, S.; Stuve, E. M. *Colloids Surf., A* **1998**, *134*, 145.
(27) Sriramulu, S.; Jarvi, T. D.; Stuve, E. M. *Electrochim. Acta* **1998**, *44*, 1127.
(28) Sriramulu, S.; Jarvi, T. D.; Stuve, E. M. *J. Electroanal. Chem.* **1999**, *467*, 132.
(29) Cherstiouk, O. V.; Simonov, P. A.; Zaikovskii, V. I.; Savinova, E. R. *J. Electroanal. Chem.* **2003**, *554*−*555*, 241.
(30) Sun, S. G.; Clavilier, J. *J. Electroanal. Chem.* **1987**, *236*, 95.
(31) Chen, D.-J.; Hofstead-Duffy, A. M.; Park, I.-S.; Atienza, D. O.; Susut, C.; Sun, S.-G.; Tong, Y. Y. J. *J. Phys. Chem. C* **2011**, *115*, 8735.
(32) Osawa, M.; Tsushima, M.; Mogami, H.; Samjeske, G.; Yamakata, A. *J. Phys. Chem. C* **2008**, *112*, 4248.
(33) Kunimatsu, K.; Hanawa, H.; Uchida, H.; Watanabe, M. *J. Electroanal. Chem.* **2009**, *632*, 109.
(34) Zeng, D.-M.; Jiang, Y.-X.; Zhou, Z.-Y.; Su, Z.-F.; Sun, S.-G. *Electrochim. Acta* **2010**, *55*, 2065.
(35) Climent, V.; Attard, G. A.; Feliu, J. M. *J. Electroanal. Chem.* **2002**, *532*, 67.

(36) Chen, Q.-S.; Solla-Gull, J.; Sun, S.-G.; Feliu, J. M. *Electrochim. Acta* **2010**, *55*, 7982.
(37) Lu, G. Q.; Chrzanowski, W.; Wieckowski, A. *J. Phys. Chem. B* **2000**, *104*, 5566.
(38) Miyake, H.; Ye, S.; Osawa, M. *Electrochem. Commun.* **2002**, *4*, 973.